INTERNATIONAL JOURNAL OF CLIMATOLOGY
Int. J. Climatol. (2017)
Published online in Wiley Online Library
(wileyonlinelibrary.com) DOI: 10.1002/joc.5214

RMetS
Royal Meteorological Society

Simulations of the observed 'jump' in the West African monsoon and its underlying dynamics using the MIT regional climate model

Eun-Soon Im[a,b,c]* and Elfatih A. B. Eltahir[d]

[a] *Center for Environmental Sensing and Modeling, Singapore-MIT Alliance for Research and Technology, Singapore*
[b] *Department of Civil and Environmental Engineering, The Hong Kong University of Science and Technology, China*
[c] *Division of Environment and Sustainability, The Hong Kong University of Science and Technology, China*
[d] *Ralph M. Parsons Laboratory, Department of Civil and Environmental Engineering, Massachusetts Institute of Technology, Cambridge, MA, USA*

ABSTRACT: The observed seasonal migration of rainfall associated with the West African monsoon (WAM) is characterized by two regimes of relatively intense rainfall: an early, intense peak over the Guinean Coast during late May to early July; and a late, less-intense peak over the Sahel during mid-July to mid-September. The transition between these two rainfall regimes occurs relatively quickly around the beginning of July. This quick transition can be described as a 'jump' of the WAM into the continent. Eltahir and Gong (1996) proposed a theory for the WAM whereby the solar radiation forcing during the summer shapes a distribution of boundary-layer entropy that peaks over the continent. By assuming a quasi-equilibrium balance between moist convection and the large-scale radiative forcing, the distribution of boundary-layer entropy can be linked to the absolute vorticity at the tropopause. According to this analytical theory, the onset of the monsoon, characterized by the 'jump', reflects of a nonlinear shift from a radiative-convective equilibrium regime to an angular momentum conserving regime that would only occur when the value of absolute vorticity in the upper troposphere approaches a threshold of zero. It is because, when the absolute vorticity is significantly different from zero, then the air as a rotating fluid is too rigid to exhibit a meridional overturning. Here, we use the MIT regional climate model (MRCM) to test this theory further and reach a couple of conclusions. First, MRCM succeeds in reproducing the main features of the observed rainfall distribution, including the 'jump'. Second, analysis of the rainfall, vorticity, entropy, and wind fields simulated by the model reveals a dynamical picture consistent with the proposed theory.

KEY WORDS West African monsoon jump; regional climate model; absolute vorticity; boundary-layer entropy

Received 20 January 2017; Revised 18 June 2017; Accepted 27 June 2017

1. Introduction

The timing of the rainy season in the Sahel is associated with the migration of the West African monsoon (WAM) into the land region. Availability of water in this region depends strongly on the WAM due to the unique geographical location of the Sahel, situated in the transition zone between wet and dry climate regimes. Therefore, improving the skill of models in predicting the WAM and related rainfall can contribute to reducing vulnerability of agriculture to climate variability in this region.

The migration of the WAM into the continent occurs in a discrete step that can be described as a 'jump' (Cook, 2015; Sultan and Janicot, 2000; Thorncroft *et al.,* 2011). Several studies based on both numerical modelling and observational analysis have been performed to enhance our understanding of the northward 'jump' of the WAM and the underlying physical and dynamical mechanisms. Hagos and Cook (2007) and Cook (2015) emphasized the role of inertial instability in the WAM 'jump', which develops as a result of strong meridional pressure gradients associated with diabatic heating differences between the coast region and the continental interior. Gu and Adler (2004) suggested that the WAM 'jump' is the result of combination of various physical factors such as the sea surface temperature (SST) meridional gradient and a northward shift of the African Easterly Jet (AEJ). Amplification of the heat low dynamics due to interaction with the Northern orography of the Atlas-Ahaggar Mountains (Sultan and Janicot, 2003) and spatial distribution of surface albedo over West Africa that drives the spatio-temporal location of the surface temperature maxima (Ramel *et al.,* 2006) are also discussed as important ingredients of the WAM dynamics. The relationships between the intra-seasonal variation of the WAM and northward migration of the Inter-Tropical Convergence Zone (ITCZ) (Sultan and Janicot, 2000) and African Easterly Waves (AEWs) (Crétat *et al.,* 2014) have also been assessed in an effort to advance the understanding of the WAM.

In particular, Eltahir and Gong (1996, hereinafter EG96) proposed a theoretical framework for

* Correspondence to: E-S. Im, Academic Building 3595, The Hong Kong University of Science and Technology, Clear Water Bay, Kowloon, Hong Kong, China. E-mail: ceim@ust.hk

describing the WAM dynamics in wet and dry years. EG96 derived the relationship between the absolute vorticity in the upper troposphere and the meridional gradient of boundary-layer entropy (see Equation (4) in EG96) on the basis of the dynamics of zonally symmetric thermally direct atmospheric circulations developed by Plumb and Hou (1992) and Emanuel (1995). Plumb and Hou (1992) demonstrated that the absolute vorticity at the upper level explains the development of a meridional circulation (an angular momentum conserving regime) in the idealized experiment with a zonally symmetric model. In particular, EG96 applies this general theory to the particular case of WAM. In this theory for the WAM, a 'jump' can be interpreted as a result of the cumulative radiation forcing that shapes a distribution of boundary-layer entropy with peaks over the continent. By assuming a moist atmosphere that satisfies a quasi-equilibrium balance between moist convection and the large-scale radiative forcing, the distribution of boundary-layer entropy can be linked to the absolute vorticity at the tropopause. More specifically, if the upper-level absolute vorticity is dominated by the planetary component (proportional to latitude) and thermal forcing is weak, there is little meridional circulation (Zheng, 1997). The meridional gradient of boundary-layer entropy plays the role of the thermal forcing that induces a relative vorticity strong enough to cancel the planetary vorticity at the tropopause. Therefore, according to this theory, the onset of the monsoon, characterized by the 'jump', is a reflection of a nonlinear shift from a radiative-convective equilibrium regime to an angular momentum conserving regime. This nonlinear process occurs when the absolute vorticity in the upper troposphere approaches a threshold of zero. Once angular momentum conserving regime becomes dominant, the meridional circulation, which is the large-scale forcing for rainfall formation, is expected to develop.

There have been subsequent studies that supported the findings of EG96. For example, Le Barbe *et al.* (2002) identify the two climatic regimes that satisfy the nonlinear monsoon concept, which is in line with the theory proposed by EG96. While Fontaine and Philippon (2000) demonstrate that the meridional distribution of energy in the boundary layer is directly related to the monsoon dynamics in West Africa, Fontaine *et al.* (1999) show that seasonal forecasting method including the meridional gradient of moist static energy as a predictor may improve the skill for rainfall forecasting over West Africa.

Moreover, EG96 itself provides the empirical evidence that proposed theoretical relation is consistent with observational analysis, showing that the magnitude of meridional gradient of entropy induced by SST anomalies off the Southern coast of West Africa is associated with rainfall variation in the Sahel region. Although EG96 provides a consistent theory to interpret the different regimes of the meridional circulation associated with the WAM, this theory was tested through analysis of observations in only a few years, representative of wet and dry years, due to limited availability of data in this region. Here, we test the dynamical constraints of WAM proposed by EG96 based on a long-term simulation using a regional climate model.

The objective of the present study is to assess whether the MIT regional climate model (MRCM) is capable of reproducing the observed rainfall 'jump' and the associated dynamics of the WAM in light of the theory proposed by EG96. Im *et al.* (2014) demonstrated that MRCM can successfully simulate the WAM with significant improvement compared to other previous versions of the same model. Based on that previous study, we extend our analysis to examine detailed characteristics of the WAM 'jump' and background dynamics using key variables such as rainfall, vorticity, wind, and entropy. Note that we do not intend to derive a new theory, but to apply the well-established theory of EG96 and check if it is valid in the context of three-dimensional climate simulations. If the dynamic constraint theoretically derived from the assumption of a zonally symmetrical atmosphere is still relevant to some extent in three-dimensional 'real' atmosphere, it will be helpful for enhancing our understanding of the WAM dynamics. Therefore, the degree of realism achieved in MRCM simulations of the WAM is fundamentally important to demonstrate the skill of MRCM as a tool to be used in both climate prediction and sensitivity studies over Africa.

2. Model and data used

In this study, MRCM is used to investigate the WAM. Based on the Regional Climate Model Version 3 (RegCM3, Pal *et al.,* 2007), MRCM maintains much of the same structure but incorporates several improvements, including coupling of the Integrated Biosphere Simulator (IBIS) land surface scheme (Winter *et al.,* 2009), a new bare-soil albedo assignment method (Marcella, 2012), new convective cloud and convective rainfall auto-conversion schemes (Gianotti and Eltahir, 2014a, 2014b), and modified boundary-layer height and boundary-layer cloud schemes (Gianotti, 2012). To investigate the impact of these newly implemented or upgraded physical schemes, Im *et al.* (2014) completed a series of experiments over West Africa, in which simulations of the WAM show a significant sensitivity to the choices of the land surface and convection schemes, which is in line with many other studies that assess the dependence of the skill of WAM simulations on model physics (e.g. Steiner *et al.,* 2009; Dominguez *et al.,* 2010; Flaounas *et al.,* 2011). Compared with the combinations of the Biosphere-Atmosphere Transfer Scheme (BATS) land surface scheme and two convection schemes (Grell with the Fritsch-Chappell closure and standard Emanuel) that are default schemes within RegCM3 (Pal *et al.,* 2007), the simulation that combines the IBIS land surface scheme and the modified Emanuel scheme shows the best performance, reflected in the simulations of rainfall, surface energy balance, and the large-scale circulation. Therefore, we adopt the same version of MRCM for this study.

Using this model, we performed two experiments: namely, control (50 km) and high-resolution (20 km) simulations. Except for the different horizontal resolutions, these experiments were performed with all other conditions being identical. The domain covers most of West Africa and the Atlantic Ocean centred at 3°W and 15°N (see Figure 1 in Im *et al.,* 2014). The initial and boundary conditions used by MRCM are specified according to the ERA-Interim reanalysis with a resolution of $1.5° \times 1.5°$ at 6-h intervals (Uppala *et al.,* 2008). The simulations span 20 years continuously from January 1989 to December 2008. Although additional spin-up time is not added, this should not introduce a significant error because (1) initial soil moisture conditions are specified from long-term offline simulations that bring soil moisture in equilibrium with the climate of the region, and (2) the analysis is focused on the warm season (May to October), which is 4 months removed from the initial conditions. The SST are prescribed by the National Oceanic and Atmospheric Administration (NOAA) Optimum Interpolation (OI) SST dataset with a horizontal resolution of $1° \times 1°$ and weekly resolution during the whole simulation period (1989–2008). Hereafter, the control and high-resolution simulations with 50 and 20 km horizontal resolutions are denoted as 'CNT', and 'HIR', respectively.

The performance of CNT over West Africa is comprehensively evaluated against various observations in Im *et al.* (2014). In general, CNT performs reasonably well with respect to the spatial distribution and seasonal variation of rainfall, surface energy balance, and the large-scale circulation over West Africa. This performance of CNT is comparable with various state-of-the-art regional climate models participating in the Coordinated Regional Downscaling Experiment in Africa (CORDEX-Africa), as reported by Nikulin *et al.* (2012). More detailed model description and validation of MRCM's CNT performance in simulating the WAM can be found in Im *et al.* (2014); therefore, we do not duplicate the same validation results in this study. Instead, we focus on the detailed characteristics of the WAM 'jump' and background dynamics based on the analysis of relevant variables at the daily time-scale.

For the analysis of dynamics of WAM presented in Section 3.2, absolute vorticity and boundary-layer entropy are calculated using HIR simulation. Since absolute vorticity is the sum of the relative vorticity and the planetary vorticity, its magnitude depends on the latitudinal displacement due to change in Coriolis parameter with respect to latitude. Following to the expression used EG96, the boundary-layer entropy is described as $c_p \times \ln \theta_e^*$. Here, c_p is specific heat capacity at constant pressure and θ_e^* is the saturated equivalent potential temperature averaged over the two lowest pressure levels (i.e. 1000 and 925 hPa), which is a function of the temperature and humidity.

For the validation of daily rainfall, we used daily data from the Tropical Rainfall Measuring Mission (TRMM) 3B42 product (Huffman *et al.,* 2007). Since TRMM data are only available from 1998, a 16-year average (1998–2013) is used.

3. Results

3.1. Characteristics of the West African monsoon 'jump'

We begin our analysis with the comparison of climatological aspects of rainfall between observation and simulations during the Northern Hemisphere summer season (June–July–August: JJA). Figure 1 presents the spatial distribution of JJA mean rainfall derived from TRMM observation and two simulations with different resolutions. The HIR and CNT simulations are averaged over the period 1989–2008 (20-year climatology) while TRMM observation is averaged over the period 1998–2013 (16-year climatology). During JJA, features common to both the observations and simulations include localized rainfall maxima offshore from the western coast of Guinea along 5°–10°N, over the Fouta-Jalon, over the Cameroon Mountains, and over the Soudano-Sahelian region including Northern Nigeria. In general, both simulations reflect reasonable model performance with respect to the spatial pattern and localized maxima. However, HIR is in quantitatively better agreement with TRMM observations in comparison to CNT, substantially reducing the dry bias seen in the CNT pattern. Nevertheless, since the improvement of HIR is limited over some regions, HIR still maintains strong underestimation of orographic rainfall maxima especially at the coast of Cameroon. Yamada *et al.* (2012) report similar differences to those simulated in CNT and HIR, and they suggest that their low resolution is not sufficient to represent the meridional circulation associated with the WAM. Yamada *et al.* (2012) conclude that the simulation of the pattern and strength of the oceanic ITCZ in the vicinity of the coastline can potentially be improved by increasing the horizontal resolution.

The reasonable performance of MRCM and the improvement achieved in HIR are more clearly revealed in simulations of the temporal evolution of the WAM. Figure 2 presents the latitude-time cross-section of 9-day running mean rainfall averaged over three different regions: the eastern Atlantic (25°–20°W), West Africa (12°W–6°E), and central Africa (15°–20°E). As in Figure 1, both simulations and TRMM observation are 20-year and 16-year climatology, respectively. The 9-day running mean is applied to smooth out high frequency fluctuations. Based on the spectral analysis of time-series of daily TRMM data (1998–2013: total of 5844 data) at random location via the Fast Fourier Transform, we did not find significant power at the periods of less than 10 days (not shown). Therefore, 9-day running mean can be justified for filtering out the high frequency noise. First, the evolution of rainfall over West Africa is quite distinguished from those of two other regions. Over the Atlantic Ocean, high-intensity rainfall greater than $13\ \mathrm{mm\ day^{-1}}$ is consistently maintained from May to October. Rainfall maxima located around 3°–5°N smoothly moves northward, reaches up to 10°N, and then retreats southward. Although the maximum intensity varies along the pathway, there is no apparent discontinuity in its northward and southward movements.

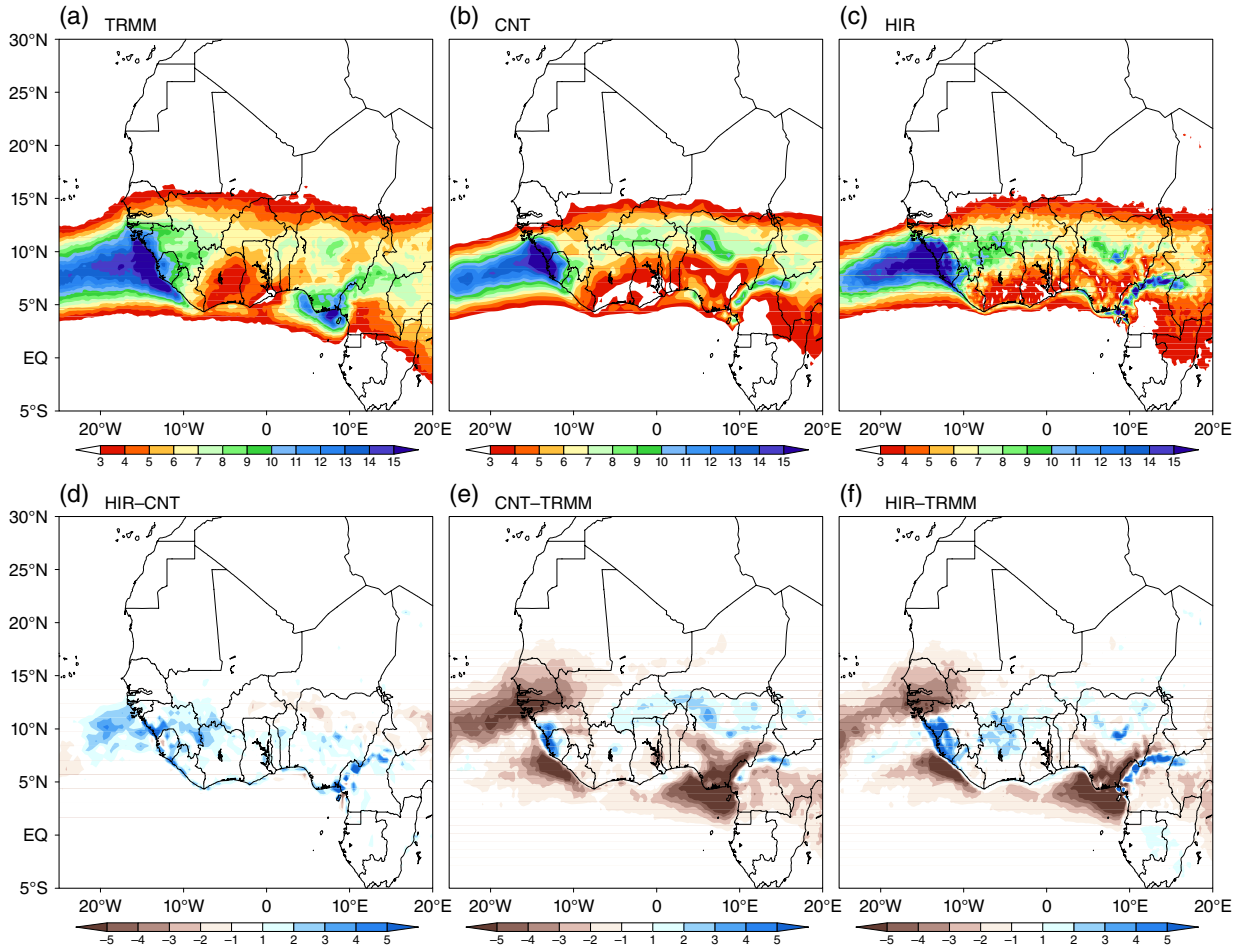

Figure 1. Spatial distribution of summer (JJA) rainfall (mm day^{-1}) from the TRMM observation (a), and CNT (b), and HIR (c) simulations, and the differences between HIR minus CNT (d), CNT minus TRMM (e), and HIR minus TRMM (f). The HIR and CNT simulations are averaged over the period 1989–2008 (20-year climatology) while TRMM observation is averaged over the period 1998–2013 (16-year climatology). [Colour figure can be viewed at wileyonlinelibrary.com].

In contrast to the Atlantic Ocean, central Africa (situated entirely over land) does not produce rainfall evolution that contains the intense and localized maxima. Rather, the intensity of rainfall is relatively weak, and a broadly spread peak appears in August. On the other hand, the temporal evolution over West Africa shows a distinct behaviour in terms of discontinuity and asymmetry of rainfall maxima. The first quasi-stationary monsoon front (leading edge of the region covered by the monsoon) appears near 5°N in late May and then 'jumps' toward the Sahel, generating a second quasi-stationary monsoon front covering 8–14°N in August, which is less intense but broader rainband compared with the first one. Due to the transitional phase from the middle of June to July, the discontinuity between the two maxima seems to be clear; this does not occur over the Atlantic Ocean to the west, nor in central Africa to the east. More importantly, the maximum rainfall over the Guinean coast is more intense and localized than that over the Sahel region, indicating an asymmetric behaviour of the WAM over the ocean and land regions.

As evidenced in Figure 2, MRCM is capable of reproducing the major characteristics of the WAM evolution similar to those in the TRMM observations. For example, both CNT and HIR successfully reproduce the monsoon 'jump'. The simulated onset timing and meridional displacement of the monsoon over the Guinean coast and the Sahel region are also realistic. However, CNT fails to capture the asymmetric behaviour of the rainfall maximum between the Guinean coast and the Sahel region. Compared to TRMM observations, CNT simulates a relatively weaker monsoon over the Guinean coast but a stronger monsoon over the Sahel, thus showing similar magnitude of the two monsoon fronts. This problem is not limited to the CNT simulation, but rather seems to be a typical error found in many other regional climate simulations over this region (Gallee *et al.,* 2004; Ramel *et al.,* 2006; Hagos and Cook, 2007; Druyan *et al.,* 2010; Sylla *et al.,* 2010b, 2013; Diaconescu *et al.,* 2015; Moukaila *et al.,* 2015). Although climate simulations using state-of-the-art models reasonably capture the climatology associated with the WAM (Gallee *et al.,* 2004; Sylla *et al.,* 2009, 2010a, 2010b; Druyan *et al.,* 2010; Xue *et al.,* 2010; Nikulin *et al.,* 2012; Hernandez-Diaz *et al.,* 2013), simulating accurate onset timing and detailed characteristics of the WAM 'jump' remains a challenge (Diallo *et al.,* 2014; Diaconescu *et al.,* 2015). Interestingly, a notable

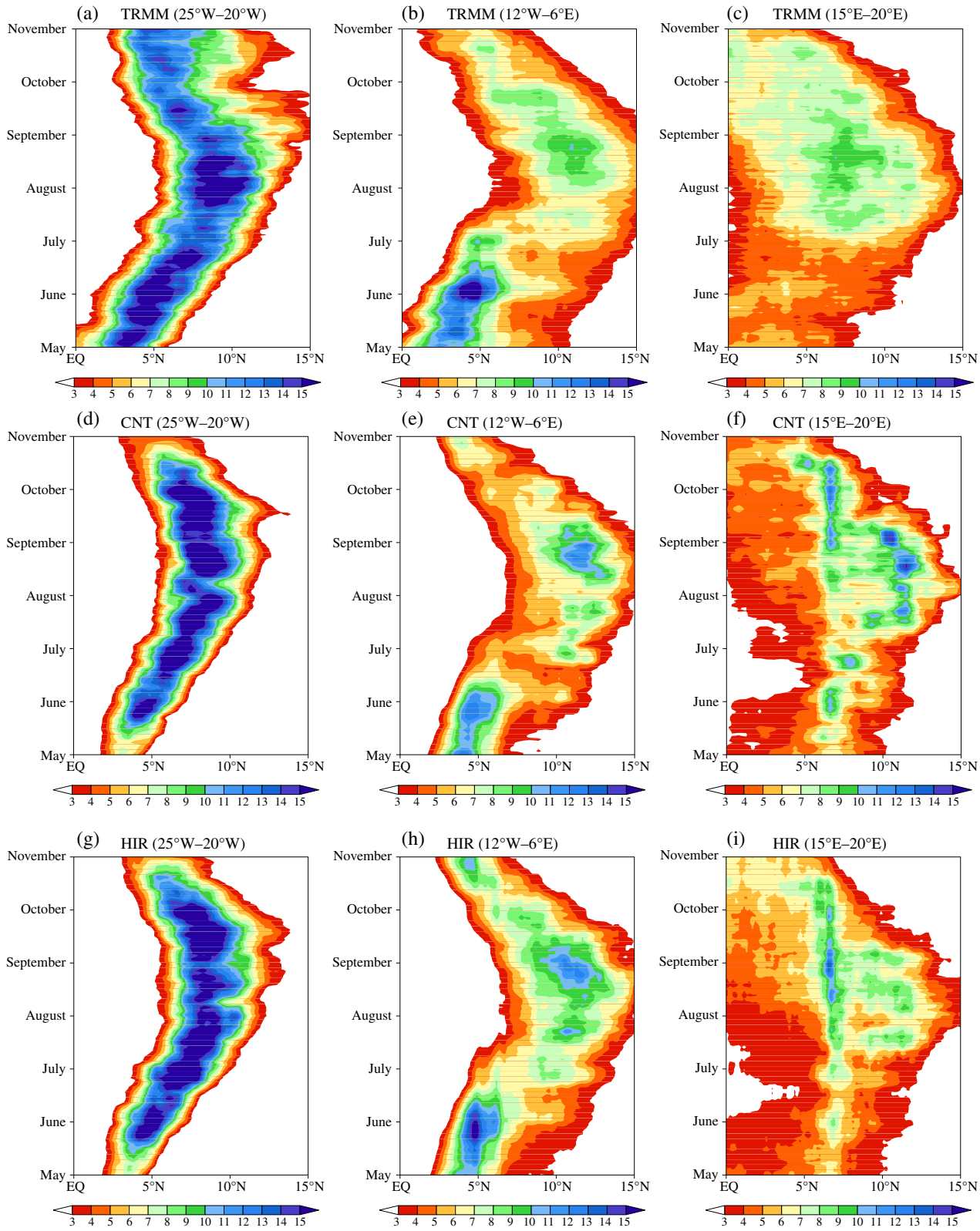

Figure 2. Latitude-time cross section of 9-day running mean rainfall (mm day^{-1}) averaged over 25°–20°W (a, d, g), 12°W–6°E (b, e, h), and 15°–20°E (c, f, i) derived from TRMM observations (a–c), and CNT (d–f) and HIR (g–i) simulations. The HIR and CNT simulations are averaged over the period 1989–2008 (20-year climatology) while TRMM observation is averaged over the period 1998–2013 (16-year climatology). Y-axis indicates from 1 May to 1 November. [Colour figure can be viewed at wileyonlinelibrary.com].

improvement is found in HIR, even without any change of physical parameterizations. The intensity of the first monsoon front simulated by HIR is indeed comparable to that of the TRMM observations, which results from the reduction in systematic dry bias along the Guinean coast. Based on our simulation, it appears that the model physics are critical for shaping general evolution patterns, including realistic positioning of the monsoon front, while a higher resolution seems to contribute to attaining its magnitude. It implicitly supports the sound physical basis of MRCM and the role of higher resolution in properly capturing the complexity of the WAM. In addition to better performance over the Guinean coast compared with CNT, and despite its deficiencies, HIR simulates a wider rainfall band (more than 3 mm day^{-1}) during the retreat period over the Atlantic Ocean and during the onset period over the Soudano-Sahelian region that closely resembles the rainfall band in TRMM observations. The superiority of HIR is also found in the central Africa region. Over this region, rainfall seems to be greatly influenced by the orography of the Cameroon Mountains. MRCM tends to exaggerate the enhancement of orographic rainfall along the Cameroon Mountains, which generates the stagnant feature maintaining suspicious local maximum around 6°–8°N. Although HIR does not solve this problem, it significantly reduces the pronounced maxima in CNT that are not observed in TRMM. This improvement might be caused by better geographical prescription (e.g. topography, land-use distribution) used in HIR with relatively high resolution.

To more quantitatively diagnose the nonlinear behaviour of the WAM, we compare the temporal evolution of area-averaged rainfall over the two target regions that correspond to the Guinean coast and the Sahel. Figure 3 displays the time-series of 9-day running mean rainfall averaged over the Guinean coast (12°W–6°E and 5°–6°N, thick line) and the Sahel region (12°W–6°E and 13°–14°N, dashed line). The selection of these sub-regions is based on a similar observation analysis that was performed by Cook (2015). Seasonality of rainfall over the Guinean coast and over the Sahel region are fairly different. Fundamentally, the rainfall series over the two regions are out of phase, reflecting the latitudinal migration of the rainfall band. While rainfall over the Sahel exhibits gradual seasonal trends, Guinean coast rainfall exhibits greater amplitude of variability with much steeper gradients. Consistent with Figure 2, the monsoon front develops over the Guinean coast in late May to early June; however, this rainfall peak rapidly declines and reaches its minimum in August. Cook (2015) also suggests that the WAM 'jump' is associated with a rapid demise in rainfall along the Guinean coast, in contrast to the smooth progression of rainfall in the Sahel.

Despite some discrepancies with the TRMM observations, both simulations by MRCM reasonably capture the distinct characteristics of intra-seasonal variation of observed rainfall over the two target regions, indicating general agreement with TRMM. Over the Guinean coast, MRCM reproduces a pattern of rainfall variability similar to the observed pattern, with a bimodal structure

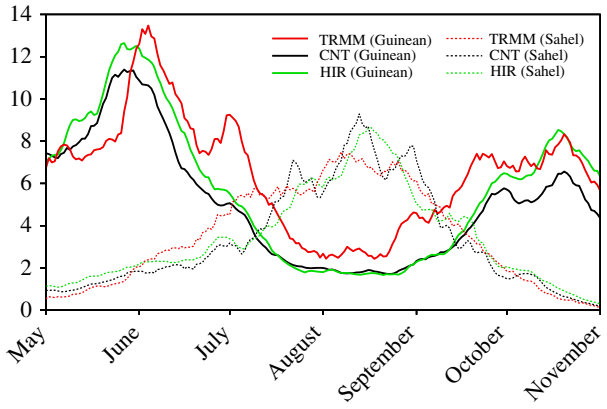

Figure 3. Time-series of 9-day running mean rainfall (mm day^{-1}) averaged over the Guinean coast (12°W–6°E and 5°–6°N, thick line) and the Sahel region (12°W–6°E and 13°–14°N, dashed line) derived from TRMM observations (red), and CNT (black) and HIR (green) simulations. The HIR and CNT simulations are averaged over the period 1989–2008 (20-year climatology) while TRMM observation is averaged over the period 1998–2013 (16-year climatology). X-axis indicates from 1 May to 1 November. [Colour figure can be viewed at wileyonlinelibrary.com].

that has two asymmetric peaks regardless of horizontal resolution. Increasing the resolution in HIR enhances the simulated amount of rainfall around the two peak periods, bringing HIR much closer to the TRMM observations. However, HIR appears to be less effective in correcting other qualitative aspects because HIR, similar to CNT, still exhibits a shift in the temporal phase with an earlier peak in May/June. Both simulations also similarly fail to capture the sub-peak observed in late June and early July. Moving to the Sahel region, MRCM generally agrees with the observations, but it tends to overestimate rainfall in the middle of August.

Although the observations and simulations show some relevant discrepancies in individual features of rainfall variability over the Guinean coast and the Sahel region, MRCM exhibits a significant skill in simulating both the timing of the monsoon onset and the associated rainfall 'jump'. For example, the first date that Sahel rainfall surpasses Guinean rainfall is simulated by MRCM fairly well in comparison to the observations. Cook (2015) notes that this 'crossing date' is somewhat subject to the choice of averaging area, statistical filtering (i.e. 9-day running mean applied in this study), and data sources. Given that this timing is an important signal for a shift in the dynamics of the WAM, the skill of MRCM in this regard – reflected in the agreement with observations of the crossing date (second week of July) – can provide an important insight on the potential for accurate simulation of the monsoon over this region.

3.2. Dynamics underlying the West African monsoon 'jump'

Accurate simulation of the WAM 'jump' in rainfall evolution is not likely without consistently accurate simulation of underlying dynamical processes. Indeed, numerous studies have demonstrated that the WAM 'jump' is

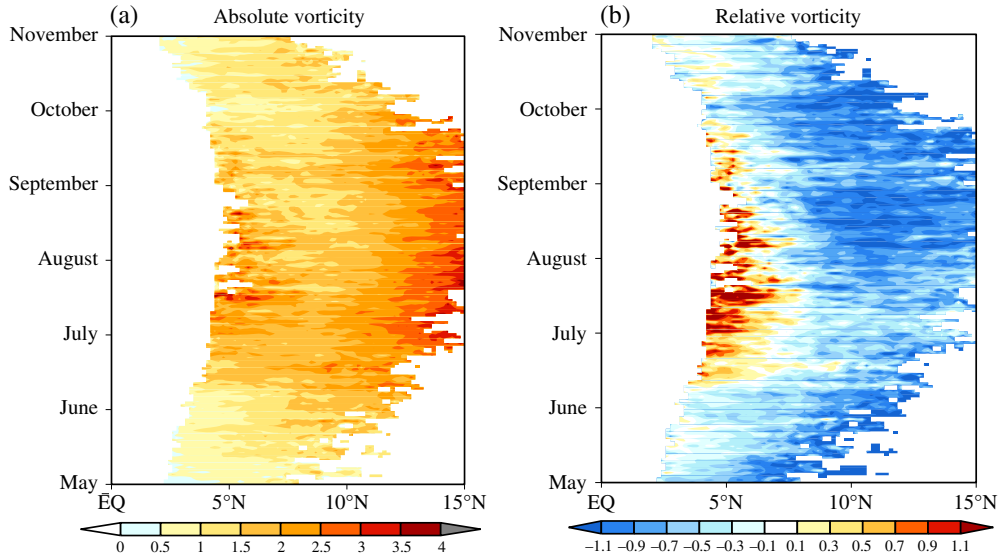

Figure 4. Latitude-time cross-section of 20-year climatological absolute (a) and relative (b) vorticity (10^{-5} s^{-1}) at 200 hPa averaged over 12°W–6°E derived from the HIR simulation. Longitudinal averaging is performed after masking out the area where rainfall is less than 5 mm day^{-1}. [Colour figure can be viewed at wileyonlinelibrary.com].

tightly connected with the dynamics of the monsoon circulation over West Africa (e.g. Druyan *et al.,* 2010; Xue *et al.,* 2010). In particular, EG96 proposed a dynamical theory of the monsoon in this region, suggesting that a vanishing absolute vorticity in the upper troposphere should lead to dominance of an angular momentum conserving regime, characteristic of the monsoon circulation. In addition, they proposed that a large meridional gradient of boundary-layer entropy forces a strong monsoon circulation, based on the theoretical relationship between circulation and entropy under the quasi-equilibrium balance between moist convection and large-scale radiative forcing. Here, we investigate whether MRCM adequately reproduce the observed relationship between circulation, absolute vorticity, and boundary-layer entropy that EG96 proposed. By comparison, despite general similarities with CNT, HIR brings some improvements in simulating the large-scale circulation (not shown), which is in line with the rainfall performance. In particular, HIR shows the better representation of monsoon dynamics proposed by EG96. To keep this paper concise, we only present the results simulated in HIR with respect to the dynamics of monsoon circulation.

Figure 4 presents the latitude-time cross section of the absolute and relative vorticity at 200 hPa averaged over West Africa (12°W–6°E) which is the same longitudinal range applied to the rainfall analysis of Figure 2. Longitudinal averaging is performed after masking out the area where rainfall is less than 5 mm day^{-1}, because we are interested in the region where the quasi-equilibrium balance is likely to be valid. First of all, the evolution of absolute vorticity seems to be correlated with that of rainfall, showing a similar discontinuous 'jump'. Relatively lower absolute vorticity (i.e. closer to zero) coincides with the first maximum of rainfall that occurs at the end of May, and the presence of relatively higher absolute vorticity is evident in the transitional phase from the middle of June to the middle of July. Therefore, this analysis is consistent with the hypothesis that near-zero values of absolute vorticity in the upper troposphere form an angular momentum conserving regime that is responsible for development of the WAM 'jump' seen in Figure 2.

However, for the second peak phase, the comparison of Figure 4(a) with Figure 2(h) reveals a mismatch between rainfall maximum and low absolute vorticity in terms of latitudinal position, in contrast with the reasonable match in the first peak phase. Minima of absolute vorticity after late July appears around 7°–8°N, but the rainfall maximum is located further north around 10°N. It is because the reasons for the relatively low absolute vorticity during the two monsoon peak periods seem to differ depending on latitude because of different magnitudes of the planetary vorticity. The latter peak reflects the variation of Coriolis parameter with respect to latitude. With only small magnitudes of relative vorticity (Figure 4(b)), absolute vorticity (defined as the sum of the planetary vorticity and the relative vorticity) reaches a low enough value for the circulation to develop during the first peak period, mainly due to the low magnitude of planetary vorticity near the coast. However, in the interior of the continent and away from the equator, the magnitude of planetary vorticity is relatively larger than that of Guinean coast. In order for the absolute vorticity to reach about zero, an equally large magnitude of negative relative vorticity has to develop in order to cancel out the planetary vorticity. Therefore, it takes a time for the solar radiation forcing to accumulate far interior of the continent until the meridional gradient of boundary-layer entropy induces relative vorticity magnitude to become strong negative value for the absolute vorticity to approach zero. After this threshold is reached, the monsoon precipitation maximum would then 'jump' into the continent. Despite of latitudinal mismatch between

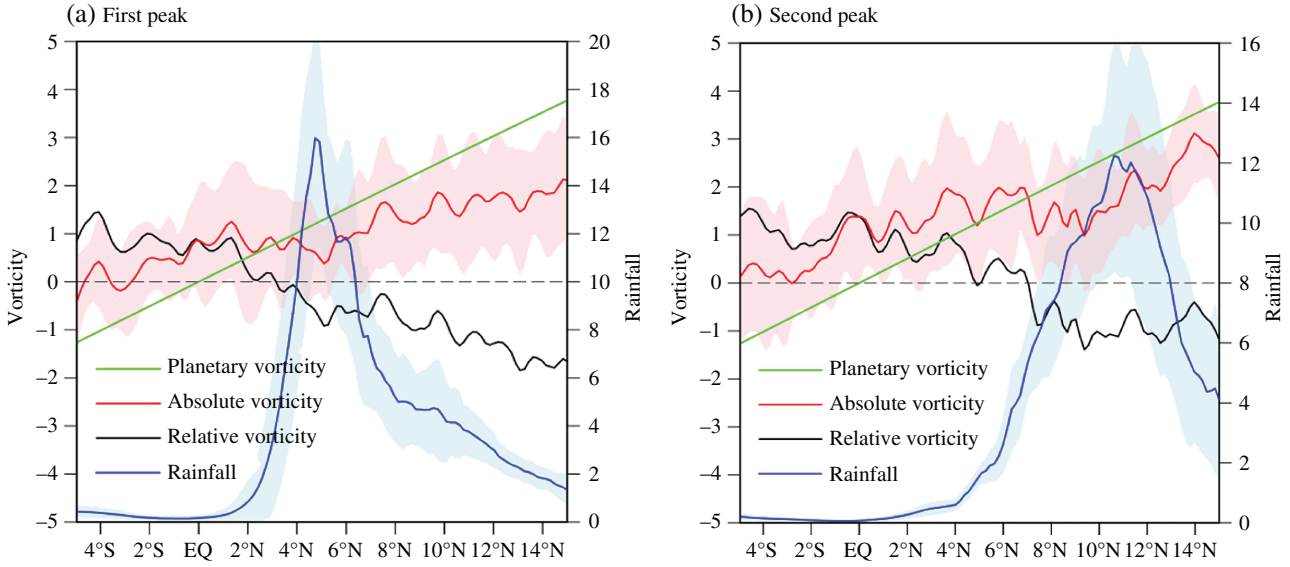

Figure 5. A 20-year climatological planetary, relative and absolute vorticity (10^{-5} s^{-1}) at 200 hPa and 2.5°E for the first (a) and second (b) peak phases derived from the HIR simulation. Rainfall (mm day^{-1}) is averaged along the Guinean coast (12°W–6°E) for the same period. The shading areas indicate ±1 standard deviation of the interannual variation of absolute vorticity (pink) and rainfall (sky blue). [Colour figure can be viewed at wileyonlinelibrary.com].

the position of rainfall maxima and the minima of absolute vorticity (see Figures 2(h) and 4(a)), the behaviour of absolute vorticity in the simulations can be viewed as a qualitative agreement between them.

To better understand the dynamical structure surrounding the first and second peak periods, we analyse the primary dynamics characteristics influencing the monsoon during the two peak periods. The first peak period is sampled from 26 May to 1 June, which corresponds to the period before the 'jump' and the simulated maximum over the Guinean coast, whereas second peak phase is selected from 26 August to 1 September, which corresponds to the period after the 'jump' and the simulated maximum over the Sahel. Since this study is focused on the WAM jump and related dynamic constraint in a climatological sense, the first and second peak periods are selected based on rainfall climatology seen in Figure 2(h) although they vary in each individual year due to interannual variation. We place our emphasis on the different behaviour of absolute vorticity in accordance with before jump, during the jump, and after the jump. Therefore, we attempt to demonstrate whether MRCM simulations agree with the theoretical dynamic constraints.

Figure 5 shows the meridional distribution of planetary, relative and absolute vorticity at 200 hPa and 2.5°E longitude for the first and second peak periods. To explicitly show how to theses dynamics are linked with rainfall variations, we also present the rainfall distribution averaged along the Guinean coast (12°W–6°E). It is clearly demonstrated that dominance of an angular momentum conserving regime appears in the monsoon peak phase over the corresponding regions. For example, the first peak phase exhibits a sudden drop in absolute vorticity and its maintenance between 4° and 6°N; this latitudinal band also coincides with the occurrence of maximum rainfall. On the other hand, the second peak phase produces an even steeper drop in absolute vorticity at around 6°N and extending up to 10°N, which corresponds with a sharp increase in rainfall to its maximum. Despite of the limited correspondence with the theory of EG96, rainfall peak appears along with relatively smaller value of the absolute vorticity. It is noted that MRCM is not an idealized zonally symmetric model, and the distinct behaviour of absolute vorticity tends to be rather obscure by taking average in temporal and spatial dimensions even though it might describe the gross features of the relation between vorticity and rainfall. However, the lower bounds for the spread given by the standard deviation of the interannual variation of absolute vorticity are likely to approach and reach zero. Therefore, this latitudinal movement of relatively low absolute vorticity is consistent with a northward shift in maximum rainfall. These simulated features complement previous observations findings that used the same analysis (see Figure 6 in EG96).

To further support the distinct behaviour of absolute vorticity between before/after jump and on jump phase, we investigate the frequency distribution of absolute vorticity, which is computed using the total 3220 values extracted from daily snapshot of corresponding period (before jump, on jump, and after jump) at individual grid points covering two target latitudinal locations (2°–6°N *vs* 7°–11°N) (Figure 6). There are much more incidences of absolute vorticity close to zero during the period before jump (i.e. first peak) and after jump (i.e. second peak) compared to transition phase (i.e. on jump). It is true that the distribution of absolute vorticity in the Guinean coast (2°–6°N) is more centred at around 0 in the first peak than in jump phase. Consistently, the distribution of jump phase over the part of Sahel (7°–11°N) is more skewed by lager positive values than that of after jump (i.e. second

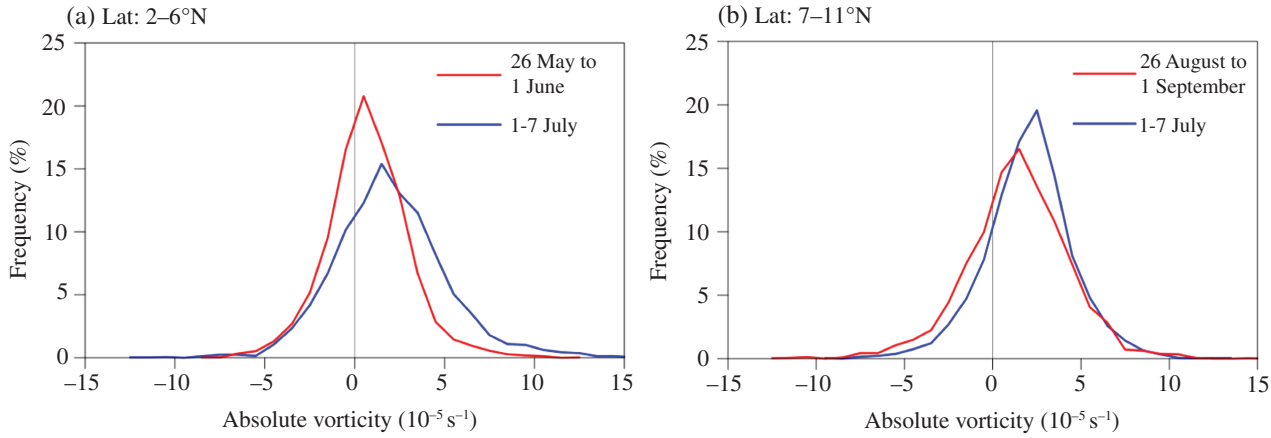

Figure 6. Frequency distribution of absolute vorticity (10^{-5} s^{-1}) pooled over 2–6°N and 7–11°N along 2.5°E for the period before jump (i.e. first peak: 26 May to 1 June), on jump (i.e. transition phase: 1–7 July) and after jump (i.e. second peak: 26 August to 1 September). Each distribution is computed using the total of 3220 values derived from temporal (daily, 7-day × 20-year) and spatial (20 km, 23 grids) dimensions. [Colour figure can be viewed at wileyonlinelibrary.com].

peak). In general, smaller values of the absolute vorticity are dominant during rainfall peak (e.g. first and second peaks), compared with that of transition phase.

To study the coupling between the monsoon dynamics in the upper troposphere (i.e. vorticity at 200 hPa in this study) with boundary-layer entropy, we present the meridional distribution of the boundary-layer entropy zonally averaged over 12°W–6°E for the first and second peak periods (Figure 7). The boundary-layer entropy reaches its maximum at different latitudinal location for the first and second peaks, extending further north for the second peak than for the first peak. More importantly, the distribution of boundary-layer entropy shows different gradients according to latitudinal displacement. The gradients of boundary-layer entropy in the corresponding latitudes where rainfall maxima occur for the first (about 2°–6°N) and second (about 6°–10°N) peaks appear to be relatively larger than other latitudes. These results are consistent with the theory of EG96 that a relatively low absolute vorticity and a large gradient of boundary-layer entropy establish favourable synoptic conditions for the development of a healthy monsoon circulation and subsequent intense rainfall over West Africa. Interannual variation as measured by standard deviation shows possible spread of yearly variations. The spread does not show large fluctuations, but it tends to slightly shrink along the latitudes with large positive gradient, implying the robust pattern with less sensitivity to years. Note that HIR shows sharp meridional gradients of temperature and humidity in boundary layer and hence entropy compared to CNT (not shown).

Finally, we focus on how northward shifts of rainfall band are tied to the large-scale characteristics through comparison of omega, vertical streamlines, absolute vorticity and divergence at 200 hPa, and the boundary-layer entropy for the first and second peaks (Figure 8). Vertical motion reflects the circulation during the two peaks, clearly showing the northward migration of deep ascending motion. Strong subsidence over the ocean contributes to low-level southerly flow that transports moisture

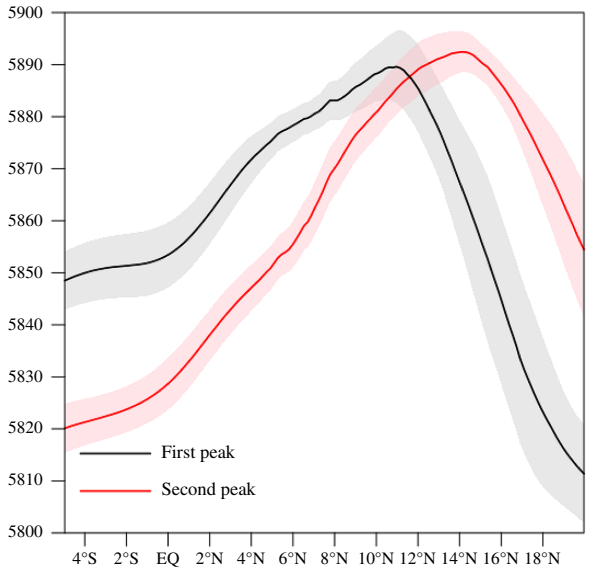

Figure 7. Meridional distribution of 20-year climatological entropy (J kg^{-1} K^{-1}) in the boundary-layer (between 1000 and 925 hPa) averaged from 12°W to 6°E for the first peak and second peak phases derived from the HIR simulation. The shading areas indicate ±1 standard deviation of the interannual variation of entropy for the first peak (grey) and second peak (pink) phases. [Colour figure can be viewed at wileyonlinelibrary.com].

from the Gulf of Guinea. During the first peak, strong ascending motion appears between 3° and 6°N over the Guinean coast, corresponding to the location of the first quasi-stationary monsoon front. Another strong ascending motion centred at 15°N is associated with dry convection in the heat low. The second peak exhibits a northward displacement of the core of upward vertical motion to 10°–12°N. Indeed, comparing vertical cross section of omega with rainfall shows the latitudinal coherence between strong ascending motion penetrating 300 hPa and maximum rain band. Vertical ascending motion also corresponds to the enhanced horizontal divergence near the upper troposphere. The movement of the region with

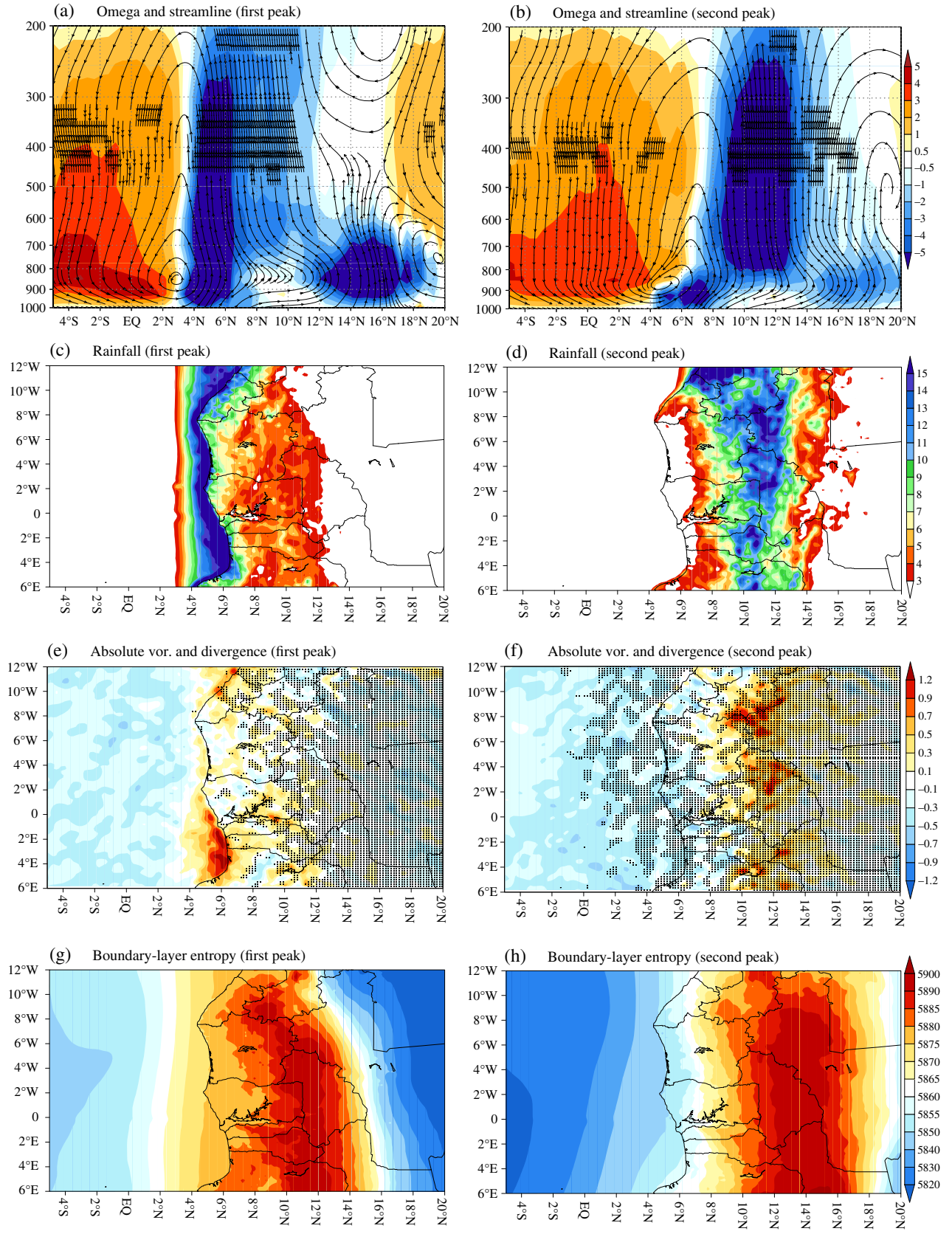

Figure 8. Vertical structure of omega (P-velocity, 10^{-5} hPa s^{-1}, shading) and streamlines combining meridional wind (m s^{-1}) and vertical wind (10^{-4} m s^{-1}) components (a, b), the spatial distribution of rainfall (mm day^{-1}: c, d), the absolute vorticity (10^{-5} s^{-1}) and divergence (10^{-5} s^{-1}, shading) at 200 hPa (e, f), and the boundary-layer entropy (J kg^{-1} K^{-1}) for the first (a, c, e, g) and second (b, d, f, h) peak phases derived from the HIR simulation. Omega in (a, b) is zonally averaged from 12°W to 6°E. Superimposed dots in (e, f) indicate the areas where the absolute vorticity is larger than 1.5×10^{-5} s^{-1}. (c–h) are rotated to facilitate the comparison in terms of latitudinal displacement. [Colour figure can be viewed at wileyonlinelibrary.com].

strong divergence at 200 hPa consistently supports the changed location of rainfall maximum between the first and second peaks. Moving to the changes in absolute vorticity, the region with smaller absolute vorticity (less than 1.5×10^{-5} s^{-1}) is shifted further northward in second peak phase than in first peak phase. Finally, it can be seen that the migration of maximum entropy region pushes the positive gradient northward. In short, large-scale dynamics and entropy in boundary layer are systematically linked with respect to rainfall jump in the West African monsoon.

4. Summary and discussion

In this study, the MRCM performance is evaluated with a focus on the reproduction of the WAM 'jump' and its underlying dynamics. The MRCM has already been tested and shown to reproduce the main climatological characteristics of the WAM through comprehensive evaluation against various observations (Im *et al.,* 2014). This study demonstrates the ability of MRCM to properly capture the WAM 'jump'. In particular, MRCM with a higher resolution has significantly improved the model's ability to simulate the intra-seasonal evolution of WAM in terms of the discontinuity and asymmetry of rainfall maxima, even without any change in physical parameterizations. In fact, the results of regional climate model simulations from the Coordinated Regional Downscaling Experiment in Africa (CORDEX-Africa, Nikulin *et al.,* 2012) and the West African Monsoon Modeling and Evaluation (WAMME, Druyan *et al.,* 2010) demonstrated that state-of-the-art regional climate models can have difficulty in accurately simulating characteristics of intra-seasonal variation of WAM rainfall such as the discontinuity and asymmetry of rainfall maxima and onset timing. Compared with them (see Figure 8 in Nikulin *et al.,* 2012 and Figure 2 in Druyan *et al.,* 2010), the MRCM HIR simulation more accurately captures the intra-seasonal variation of WAM.

There are several studies that attempt to find the relevant dynamic factors influencing the rainfall variability of the WAM, including the maximum rainfall 'jump'. In this study, we focus on the theory of EG96 that interprets the WAM 'jump' as a reflection of a nonlinear shift from a radiative-convective equilibrium regime to an angular momentum conserving regime. The theory developed by EG96 is an analytical theory that explicitly links the absolute vorticity in the upper troposphere to the development of a meridional circulation (an angular momentum conserving regime). When the absolute vorticity is significantly different from zero, then the air as a rotating fluid is too rigid to exhibit a meridional overturning. In other word, only if forcing (e.g. meridional gradient of boundary-layer entropy in our study) is strong enough for induced relative vorticity to cancel the planetary vorticity, a meridional circulation exists. Therefore, when the absolute vorticity approaches zero, the theory predicts that the system would switch (jump) from a radiative-convective equilibrium regime to the angular momentum conservative regime. MRCM simulations consistently display the relationship between vorticity at upper-tropospheric levels and boundary-layer entropy that EG96 demonstrated through analysis of observations. It is clearly demonstrated that dominance of an angular momentum conserving regime (i.e. maintenance of lower absolute vorticity) appears in the monsoon peak phase over the corresponding regions (i.e. the first peak phase along the Guinean coast and the second peak phase in the Sahel). Furthermore, a relatively larger gradient of boundary-layer entropy appears in the corresponding latitudes for the first and second peaks with rainfall maxima and lower absolute vorticity. Therefore, MRCM simulations support the theory of EG96 that a relatively low absolute vorticity in the upper troposphere and a large gradient of boundary-layer entropy are important ingredients for the onset of the monsoon and for maintaining a healthy monsoon circulation.

However, we acknowledge that the simulations show some discrepancies from the theory that was analytically derived. In order to develop an analytical theory, EG96 and Plumb and Hou (1992) had to assume zonal symmetry. West Africa is close to that assumption; however, does not fit perfectly. So strictly speaking the theory is only approximately valid when tested in the context of an atmosphere that is not perfectly zonally symmetrical. Hence in Figure 6 we show that at the times of the jump, the frequency distributions of the absolute vorticity from the simulations are centred around zero, not always exactly zero but close. The tests of the theory are presented further in Figures 4 and 5. Taking these figures together, the theory seems to roughly explain the simulations, including the jump, though significant discrepancies are present.

The reasonable simulation of the WAM 'jump' and its underlying dynamics achieved by MRCM is a significant step in illustrating the skill of this model in simulating the WAM. We believe that the improved performance of MRCM presented in this study underscores its potential as a tool for practical applications such as studies of land–atmosphere interactions, climate change projections, and seasonal prediction of WAM rainfall over West Africa.

Acknowledgements

This research is supported by the National Research Foundation Singapore under its Campus for Research Excellence and Technological Enterprise programme. The Center for Environmental Sensing and Modeling is an interdisciplinary research group of the Singapore-MIT Alliance for Research and Technology. The first author was partly supported by the Korea Agency for Infrastructure Technology Advancement (KAIA) grant funded by the Ministry of Land, Infrastructure and Transport (Grant 17AWMP-B083066–04). We are grateful to Dr Ross E. Alter for carefully proofreading our manuscript.

References

Cook KH. 2015. Role of inertial instability in the West African monsoon jump. *J. Geophys. Res.* **120**: 3085–3102. https://doi.org/10.1002/2014JD022579.

Crétat J, Vizy EK, Cook KH. 2014. How well are daily intense rainfall events captured by current climate models over Africa. *Clim. Dyn.* **42**: 2691–2711.

Diaconescu EP, Gachon P, Scinocca J, Laprise R. 2015. Evaluation of daily precipitation statistics and monsoon onset/retreat over western Sahel in multiple datasets. *Clim. Dyn.* **45**: 1325–1354.

Diallo I, Bain CL, Gaye AT, Moufouma-Okia W, Niang C, Dieng MDB, Graham R. 2014. Simulation of the West African monsoon onset using the HadGEM3-RA regional climate model. *Clim. Dyn.* **43**: 575–594.

Dominguez M, Gaertner MA, de Rosnay P, Losada T. 2010. A regional climate model simulation over West Africa: parameterization tests and analysis of land-surface files. *Clim. Dyn.* **35**: 249–265.

Druyan LM, Feng J, Cook KH, Xue Y, Fulakeza M, Hagos SM, Konaré A, Moufouma-Okia W, Rowell DP, Vizy EK, Ibrah SS. 2010. The WAMME regional model intercomparison study. *Clim. Dyn.* **35**: 175–192.

Eltahir EAB, Gong C. 1996. Dynamics of wet and dry years in West Africa. *J. Clim.* **9**: 1030–1042.

Emanuel KA. 1995. On thermally direct circulation in moist atmospheres. *J. Atmos. Sci.* **52**: 1529–1534.

Flaounas E, Bastin S, Janicot S. 2011. Regional climate modeling of the 2006 West African monsoon: sensitivity to convection and planetary boundary layer parameterization using WRF. *Clim. Dyn.* **36**: 1083–1105.

Fontaine B, Philippon N. 2000. Seasonal evolution of boundary layer heat content in the West African monsoon from the NCEP/NCAR reanalysis (1968-1998). *Int. J. Climatol.* **20**: 1777–1790.

Fontaine B, Philippon N, Camberlin P. 1999. An improvement of June-September rainfall forecasting in the Sahel based upon region April-May moist static energy content (1968-1997). *Geophys. Res. Lett.* **26**: 2041–2044.

Gallee H, Moufouma-Okia W, Bechtold P, Brasseur O, Dupays I, Marbaix P, Messager C, Ramel R, Lebel T. 2004. A high-resolution simulation of a West African rainy season using a regional climate model. *J. Geophys. Res.* **109**: D05108. https://doi.org/10.1029/2003JD004020.

Gianotti RL. 2012. *Regional Climate Modeling over the Maritime Continent: Convective Cloud and Rainfall Processes*. PhD dissertation, Massachusetts Institute of Technology, 306 pp.

Gianotti RL, Eltahir EAB. 2014a. Regional climate modeling over the Maritime Continent. Part I: new parameterization for convective cloud fraction. *J. Clim.* **27**: 1488–1503.

Gianotti RL, Eltahir EAB. 2014b. Regional climate modeling over the Maritime Continent. Part II: new parameterization for autoconversion of convective rainfall. *J. Clim.* **27**: 1504–1523.

Gu G, Adler RF. 2004. Seasonal evolution and variability associated with the West African monsoon system. *J. Clim.* **17**: 3364–3377.

Hagos SM, Cook KH. 2007. Dynamics of the West African monsoon jump. *J. Clim.* **20**: 5264–5284.

Hernandez-Diaz L, Laprise R, Sushama L, Martynov A, Winger K, Dugas B. 2013. Climate simulation over CORDEX Africa domain using the fifth-generation Canadian regional climate model (CRCM5). *Clim. Dyn.* **40**: 1415–1433.

Huffman GJ, Adler RF, Bolvin DT, Gu G, Nelkin EJ, Bowman KP, Hong Y, Stocker EF, Wolff DB. 2007. The TRMM multisatellite precipitation analysis (TMPA): quasi-global, multiyear, combined-sensor precipitation estimates at fine scales. *J. Hydrometeorol.* **8**: 38–55.

Im ES, Gianotti RL, Eltahir EAB. 2014. Improving simulation of the West African monsoon using the MIT regional climate model. *J. Clim.* **27**: 2209–2229.

Le Barbe L, Lebel T, Tapsoba D. 2002. Rainfall variability in West Africa during the years 1950–90. *J. Clim.* **15**: 187–202.

Marcella MP. 2012. *Biosphere-Atmosphere Interactions over Semi-arid Regions: Modeling the Role of Mineral Aerosols and Irrigation in the Regional Climate System*. PhD dissertation, Massachusetts Institute of Technology, 282 pp.

Moukaila MS, Abiodun BJ, Omotosho JB. 2015. Assessing the capability of CORDEX models in simulating onset of rainfall in West Africa. *Theor. Appl. Climatol.* **119**: 255–272.

Nikulin G, Jones C, Giorgi F, Asrar G, Buchner M, Cerezo-Mota R, Christensen OB, Deque M, Fernandez J, Hansler A, Van Meijgaard E, Samuelsson P, Sylla MB, Sushama L. 2012. Rainfall climatology in an ensemble of CORDEX-Africa regional climate simulations. *J. Clim.* **25**: 6057–6078.

Pal JS, Giorgi F, Bi X, Elguindi N, Solmon F, Gao X, Rauscher SA, Francisco R, Zakey A, Winter J, Ashfaq M, Syed FS, Bell JL, Diffenbaugh N, Karmacharya J, Konare A, Martinez D, Da Rocha RP, Sloan LC, Steiner AL. 2007. The ICTP RegCM3 and RegCNET: regional climate modeling for the developing world. *Bull. Am. Meteorol. Soc.* **88**: 1395–1409.

Plumb RA, Hou AY. 1992. The response of a zonally symmetric atmosphere to subtropical thermal forcing: threshold behavior. *J. Atmos. Sci.* **49**: 1790–1799.

Ramel R, Gallee H, Messager C. 2006. On the northward shift of the West African monsoon. *Clim. Dyn.* **26**: 429–440.

Steiner AL, Pal JS, Rauscher SA, Bell JL, Diffenbaugh NS, Boone A, Sloan LC, Giorgi F. 2009. Land surface coupling in regional climate simulations of the West African monsoon. *Clim. Dyn.* **33**: 869–892.

Sultan B, Janicot S. 2000. Abrupt shift of the ITCZ over West Africa and intra-seasonal variability. *Geophys. Res. Lett.* **27**: 3353–3356. https://doi.org/10.1029/1999GL011285.

Sultan B, Janicot S. 2003. The West African monsoon dynamics. Part II: the "Preonset" and "onset" of the summer monsoon. *J. Clim.* **16**: 3407–3427.

Sylla MB, Gaye AT, Pal JS, Jenkins GS, Bi X. 2009. High resolution simulations of West African climate using regional climate model (RegCM3) with different lateral boundary conditions. *Theor. Appl. Climatol.* **98**: 293–314.

Sylla MB, Coppola E, Mariotti L, Giorgi F, Ruti PM, Dell'Aquila A, Bi X. 2010a. Multiyear simulation of the African climate using a regional climate model (RegCM3) with the high resolution ERA-interim reanalysis. *Clim. Dyn.* **35**: 231–247.

Sylla MB, Dell'Aquila A, Ruti PM, Giorgi F. 2010b. Simulation of the intraseasonal and the interannual variability of rainfall over West Africa with RegCM3 during the monsoon period. *Int. J. Climatol.* **30**: 1865–1883.

Sylla MB, Giorgi F, Coppola E, Mariotti L. 2013. Uncertainties in daily rainfall over Africa: assessment of gridded observation products and evaluation of a regional climate model simulation. *Int. J. Climatol.* **33**: 1805–1817.

Thorncroft CD, Nguyen H, Zhang C, Peyrille P. 2011. Annual cycle of the West African monsoon: regional circulations and associated water vapour transport. *Q. J. R. Meteorol. Soc.* **137**: 129–147.

Uppala S, Dee D, Kobayashi S, Berrisford P, Simmons A. 2008. Towards a climate data assimilation system: status update of ERAInterim. *ECMWF Newsl.* **115**: 12–18.

Winter JM, Pal JS, Eltahir EAB. 2009. Coupling of integrated biosphere simulator to regional climate model version 3. *J. Clim.* **22**: 2743–2756.

Xue Y, De Sales F, Lau WKM, Boone A, Feng J, Dirmeyer P, Guo Z, Kim KM, Kitoh A, Kumar V, Poccard-Leclercq I, Mahowald N, Moufouma-Okia W, Pegion P, Rowell DP. 2010. Intercomparison and analyses of the climatology of the West African monsoon in the West African monsoon modeling and evaluation project (WAMME) first model intercomparison experiment. *Clim. Dyn.* **35**: 3–27.

Yamada TJ, Kanae S, Oki T, Hirabayashi Y. 2012. The onset of the West African monsoon simulated in a high-resolution atmospheric general circulation model with reanalyzed soil moisture fields. *Atmos. Sci. Lett.* **13**: 103–107.

Zheng X. 1997. *Moist zonally-Symmetric Models and Their Applications to West African Monsoons*. PhD dissertation, Massachusetts Institute of Technology, 217 pp.